Supplementary Information

Out-of-plane quadrupolar excitons in Ruddlesden-Popper perovskites: theoretical insights into effects of organic spacer cations

Qingjie Feng[1], Xu Zhang[2,*], Guangjun Nan[1,*]

[1] Department of Physics, Zhejiang Normal University, Jinhua, Zhejiang 321004, P. R. China

[2] Department of Physics and Astronomy, California State University Northridge, Northridge, California 91330-8268, United States

*Corresponding authors: E-mail: xu.zhang@csun.edu; gjnan@zjnu.edu.cn

This file includes

Texts S1 to S2

Figs S1 to S11

Text S1. Formalism of time-dependent density functional theory method

In this work, we employ a newly developed first-principles method to compute the excited states that is based on linear-response time-dependent density functional theory (TDDFT) with optimally tuned (OT),[1, 2] screened and range-separated hybrid (SRSH) exchange-correlation (XC) functionals.[3-6] Unlike the traditional TDDFT methods with local and semi-local XC functionals, the TDDFT-OT-SRSH method can capture the long-range electron-electron and electron-hole interactions in solids correctly by choosing appropriate parameters, and has been extensively used to study optical and excitonic properties in solids and vdW bilayers.[7-16] Formulated with spinor wavefunctions,[17] the TDDFT-OT-SRSH method can also capture noncollinear magnetism, including spin-orbital coupling (SOC). In this method, the following non-Hermitian eigenvalue equation is solved to determine the exciton energies and wavefunctions:[18]

$$\begin{pmatrix} A & B \\ B^* & A^* \end{pmatrix}\begin{pmatrix} X_I \\ Y_I \end{pmatrix} = \omega_I \begin{pmatrix} 1 & 0 \\ 0 & -1 \end{pmatrix}\begin{pmatrix} X_I \\ Y_I \end{pmatrix} \tag{S1}$$

where the pseudo-eigenvalue ω_I represents the I-th exciton energy. The matrix elements of $\boldsymbol{A}$ and $\boldsymbol{B}$ in the basis of two-component spinor orbitals ($ij\sigma$) are given by:

$$A_{ij\sigma,kl\tau} = \delta_{i,k}\delta_{j,l}(\varepsilon_j - \varepsilon_i) + K_{ij,kl} \tag{S2}$$

$$B_{ij,kl} = K_{ij,lk}. \tag{S3}$$

Here, K is the coupling matrix where indices i and k indicate the occupied Kohn-Sham (KS) orbitals, and j and l represent the virtual KS orbitals. According to the assignment ansatz of Casida, the many-body wavefunction of an excited state I can be written as

$$\Phi_I \approx \sum_{ij\sigma} \frac{X_{I,ij\sigma} + Y_{I,ij\sigma}}{\sqrt{\omega_I}} \hat{a}_{j\sigma}^{\dagger}\hat{a}_{i\sigma}\Phi_0 = \sum_{ij\sigma} Z_{I,ij}\hat{a}_{j\sigma}^{\dagger}\hat{a}_{i\sigma}\Phi_0 , \tag{S4}$$

where $Z_{I,ij} = (X_{I,ij} + Y_{I,ij})/\sqrt{\omega_I}$; $\hat{a}_{i\sigma}$ is the annihilation operator acting on the *i*-th KS orbital with spin σ, and Φ_0 is the ground-state many-body wavefunction taken to be the single-Slater determinant of the occupied KS orbitals. Based on the many-body wavefunctions, we can calculate the charge density associated with the exciton states as[19]

$$\rho_I = \sum_{ijj'} Z^*_{I,ij} Z_{I,ij'} \phi^*_j \phi_{j'} - \sum_{ii'j} Z^*_{I,ij} Z_{I,i'j} \phi^*_{i'} \phi_i \quad , \tag{S5}$$

where ϕ_i is KS orbital. In order to reduce the computational cost associated with the Fock-like exchange on large systems, the first-order perturbation theory to the range-separated hybrid Kohn-Sham Hamiltonian is used.[20]

In this noncollinear (TD)DFT-OT-SRSH method, there are three parameters α, β and γ that need to be specified. α determines the contribution from the exact exchange and β controls the contribution from the long-range exchange terms. γ is the range-separation parameter. α and β satisfy the requirement of $\alpha+\beta=1/\varepsilon_0$ where ε_0 is the scalar dielectric constant of the solid. According to the high-frequency dielectric constant calculated in this work (Figure 3b), the optimal set of the parameters (α=0.21, ε_0=4.0 and γ=0.1) is determined for $(PEA)_2PbI_4$. With these parameters, the calculated fundamental bandgap (E_g) and optical bandgap (E_{opt}) is 2.60 eV and 2.20 eV, respectively. The binding energy (E_b) is 0.40 eV. These values agree well with the experimentally reported fundamental bandgap (E_g = 2.57 ~ 2.65 eV) and optical bandgap (E_{opt} = 2.3 ~ 2.4 eV)[21, 22] as well as the binding energy (E_b = 0.16~0.45 eV)[23].

Text S2. Formalism of oscillator strength of exciton

To obtain the optical dipole moment for an exciton, we first determine the single-particle electron-hole transitions involved in the exciton. As mentioned above, the many-body wavefunction of the

exciton Φ_I is expressed as a linear combination of the single-particle electron-hole transitions, and $Z_{I,ij}$ represents the corresponding electron-hole transition amplitude. The polarization-dependent optical dipole moment (μ_I) of the exciton *I* is calculated as

$$\mu_I = \sum_{i,j,\sigma} Z_{I,ij} P_{ij} \tag{S6}$$

$$P_{ij} = \langle \phi_i | \hat{\varepsilon} r | \phi_j \rangle \tag{S7}$$

where P_{ij} is the transition dipole moment between the KS occupied state ϕ_i and unoccupied state ϕ_j. $\hat{\varepsilon}$ is the unit vector of the electric field of the polarized light, and **r** is the position operator of the electron. Since the position operator **r** is ill-defined in the periodic boundary conditions, we employ the velocity operator $i[H,r] = p + i[V_{NL},r]$ to compute the transition dipole moment,[24, 25] where *p* is the momentum operator and V_{NL} is the nonlocal pseudopotential. Considering that the errors by neglecting the commutator of nonlocal pseudopotential can be significantly reduced by including d-projectors in the PAW potential,[26, 27] we have omitted such commutator and only consider the momentum operator in the calculation of the transition dipole moment. The oscillator strength is then determined by

$$f = \frac{2m_e\omega_I}{3\hbar^2}{\mu_I}^2 \tag{S8}$$

where m_e is the mass of the electron and ħ is the reduced Planck constant.

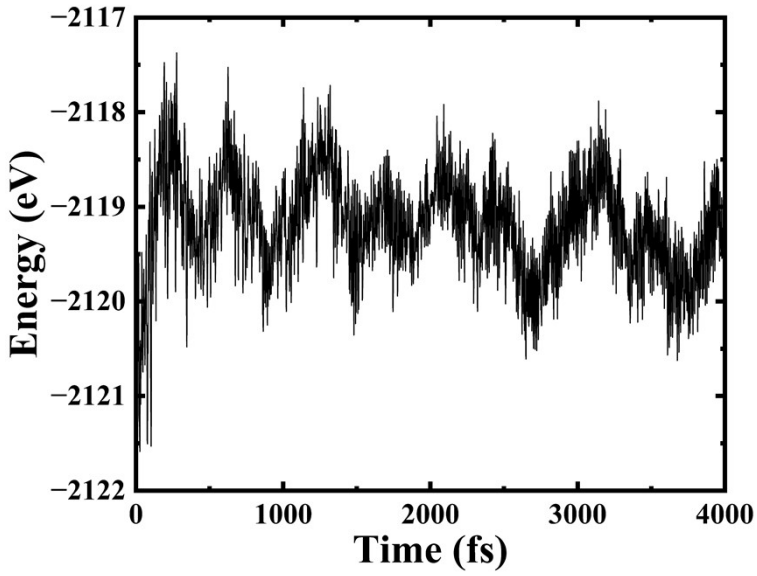

Figure S1. The change of ground-state energy during the ab initio molecular dynamics simulation at 300 K.

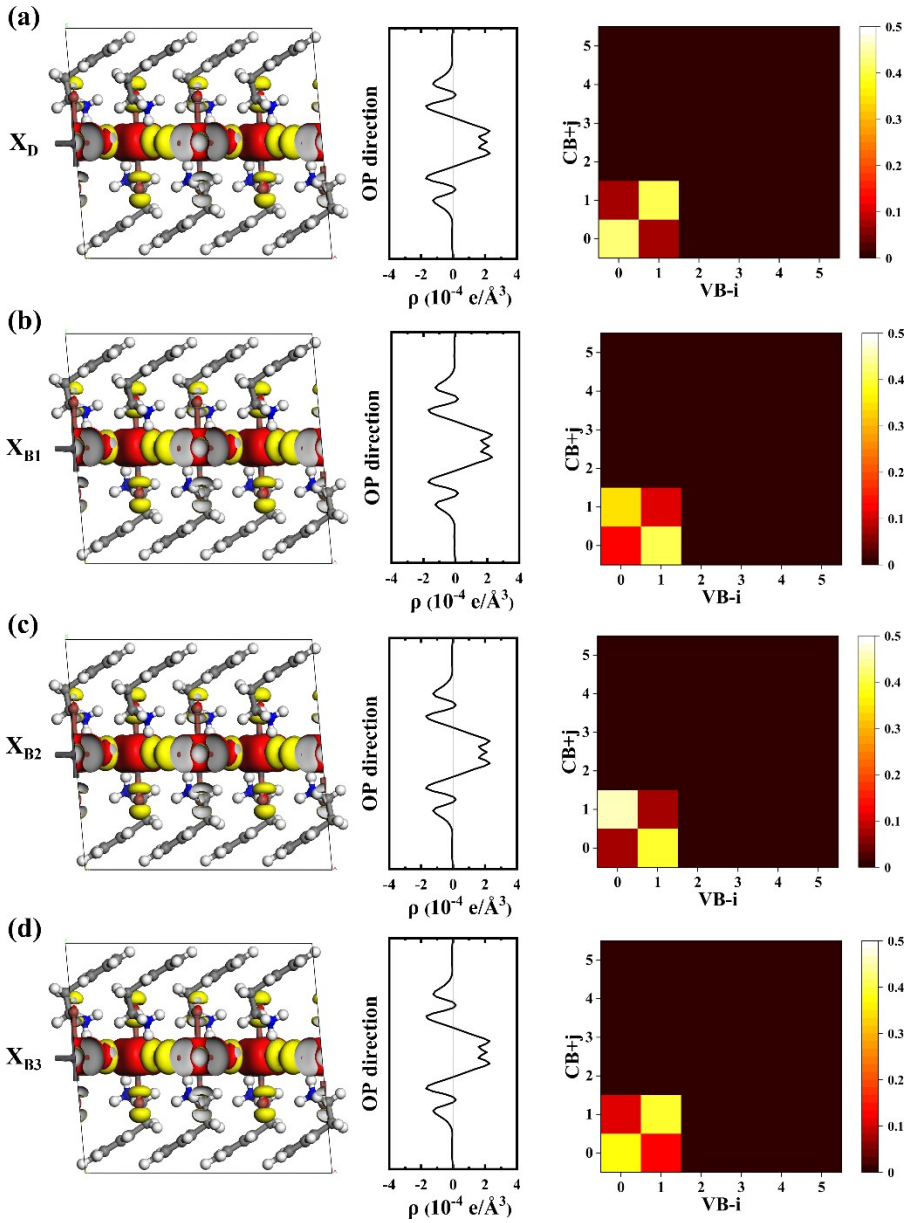

Figure S2. Exciton charge distributions in 3D lattice (left panel) and along OP direction (middle panel) as well as transition amplitude analysis (right panel) for (a) X_D, (b) X_{B1}, (c) X_{B2}, (d) X_{B3} exciton states. For the figures in the left panel, the electron and hole densities are shown in red and yellow with the iso-surface value being 1.0×10^{-3} e/Å^3, respectively. For the figures in the right panel, the single-particle orbitals below (above) valence (conduction) band edge are defined as VB-i (CB+j) in the horizontal and vertical coordinate with i (j) being the integer.

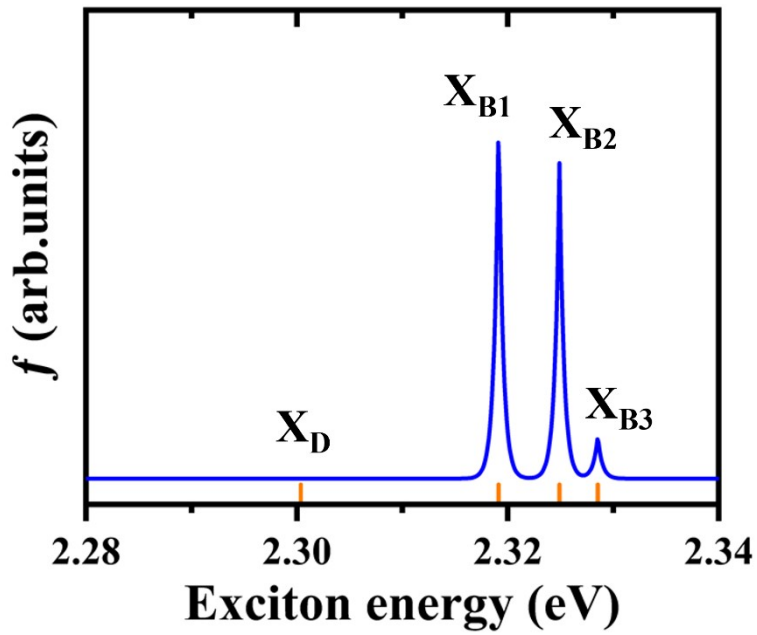

Figure S3. Exciton oscillator strength (*f*) with orange bars representing excitonic energy levels of X_D, X_{B1}, X_{B2} and X_{B3} exciton states based on the geometric structure used in Figure 2c.

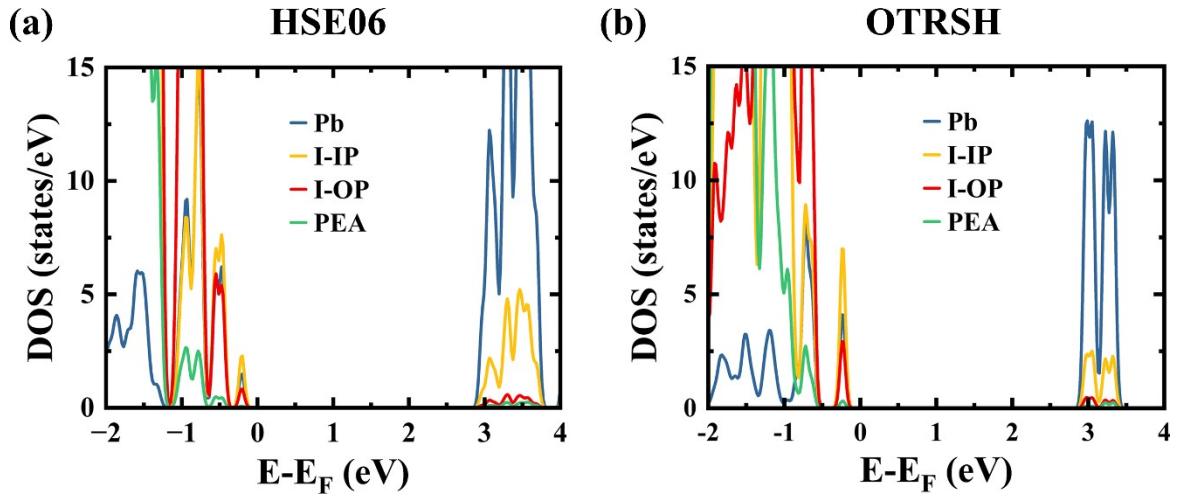

Figure S4. DOS of $(PEA)_2PbI_4$-(1) phase calculated by adopting (a) HSE06 and (b) OT-SRSH XC functionals.

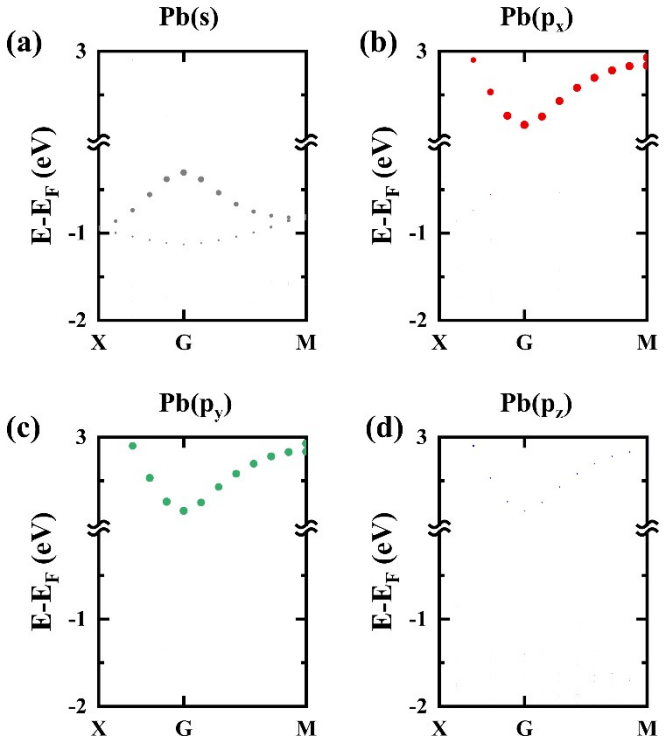

Figure S5. Energy bands of (a) s orbital, (b) p_x orbital, (c) p_y orbital and (d) p_z orbital of Pb ions in $(PEA)_2PbI_4$-(1) phase calculated at HSE06+SOC level of theory.

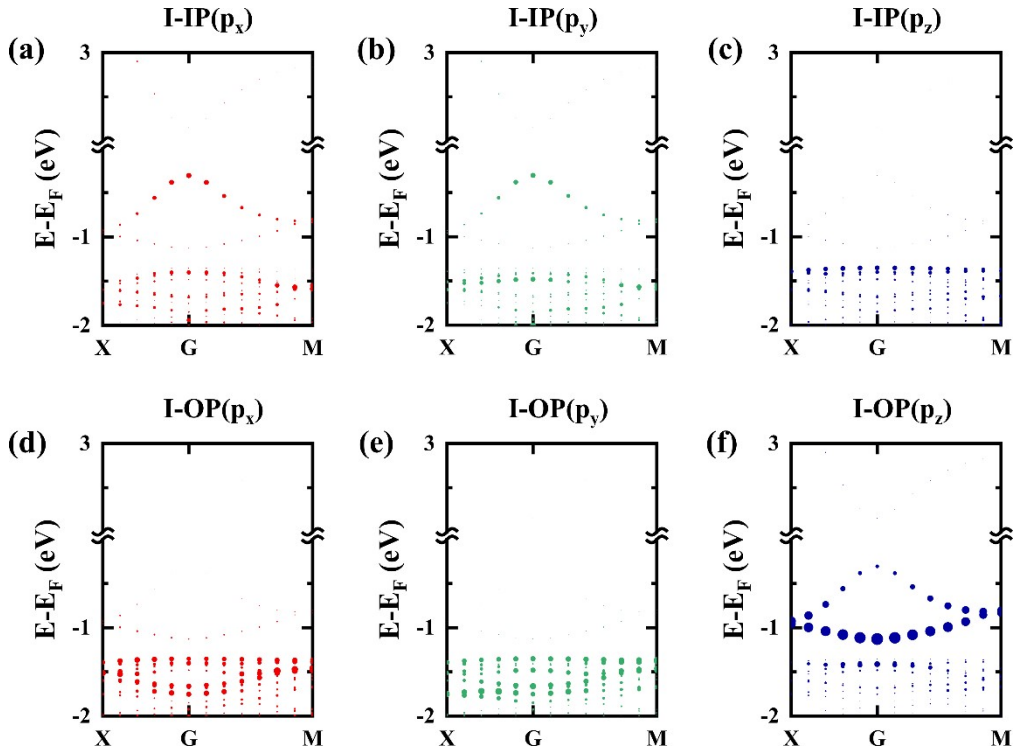

Figure S6. Energy bands calculated at the HSE06+SOC level of theory for I ions at equatorial and apical positions in $(PEA)_2PbI_4$-(1) phase. (a-c) Energy bands of p_x, p_y and p_z orbitals of equatorial I ions; (d-f) Energy bands of p_x, p_y and p_z orbitals of apical I ions.

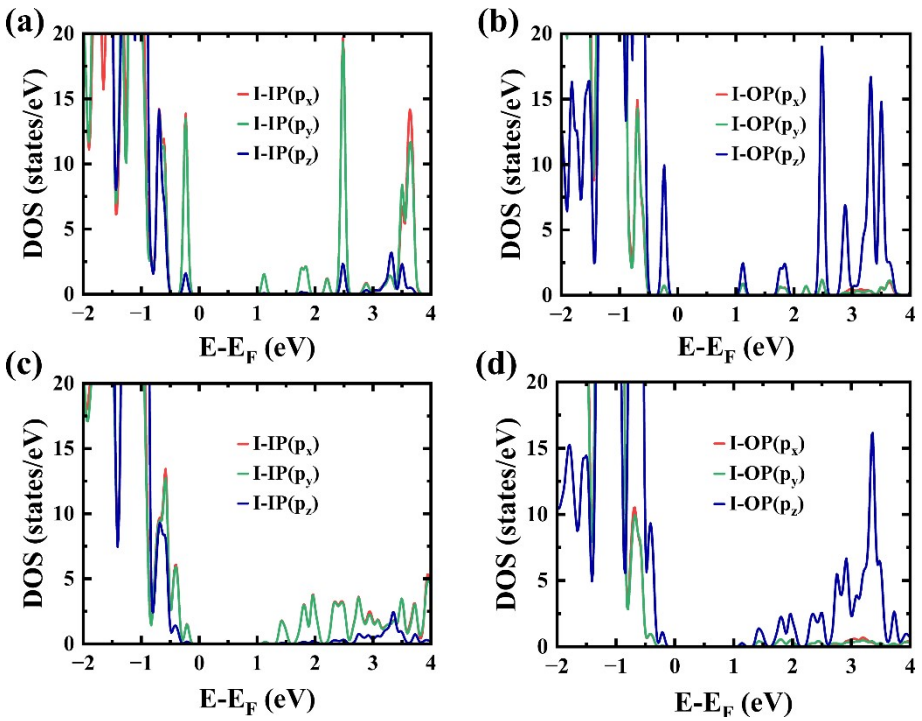

Figure S7. Partial DOS of the supercells of $(PEA)_2PbI_4$-(1) phase calculated at PBE+SOC level of theory. (a, b) Partial DOS by sampling the Brillouin zone at Γ point for the I species at the equatorial and apical sites, respectively. (c, d) Partial DOS by sampling the Brillouin zone with 5◊5x1 k-point mesh for the I species at the equatorial and apical sites, respectively.

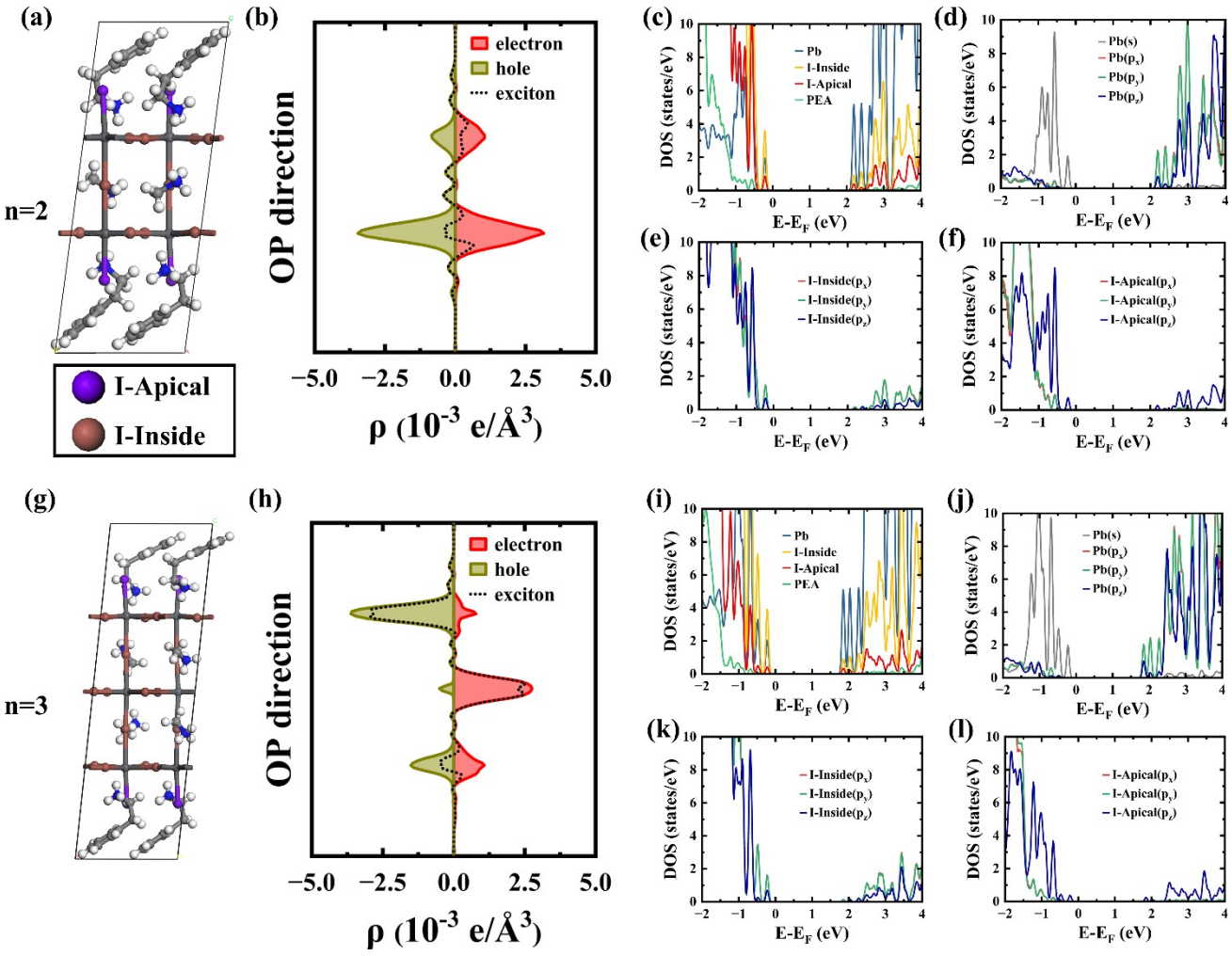

Figure S8. Electronic and excitonic properties of $(PEA)_2(MA)_{n-1}Pb_nI_{3n+1}$-(1) ($n$ = 2 and 3) RPPs. (a, g) Definition for the apical I ions at the outermost of the inorganic sublattice (I-Apical) and the I ions locating inside the inorganic sublattice (I-Inside) for n = 2 and 3. (b, h) Photoexcited electron and hole densities (shaded regions) as well as the corresponding exciton densities along the OP direction (dotted line). (c, i) DOS for Pb ions, I-Inside ions, I-Apical ions, as well as PEA cations. (d, j) DOS resulting from s, p_x, p_y and p_z orbitals of Pb ions. (e, k) DOS for p_x, p_y and p_z orbitals of I-Inside ions. (f, l) DOS for p_x, p_y and p_z orbitals of I-Apical ions.

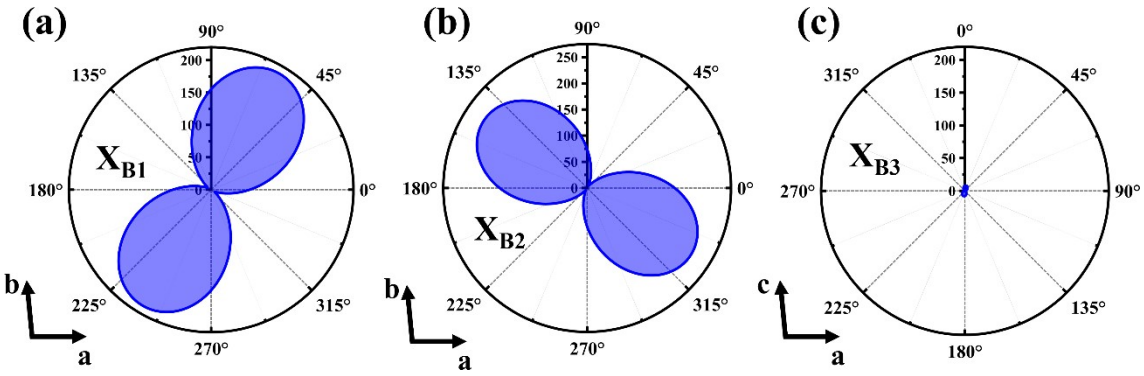

Figure S9. The oscillator strength as a function of transition dipole polarization direction for (a) X_{B1}, (b) X_{B2} and (c) X_{B3} exciton state of the stretched $(PEA)_2PbI_4$-(1) structure.

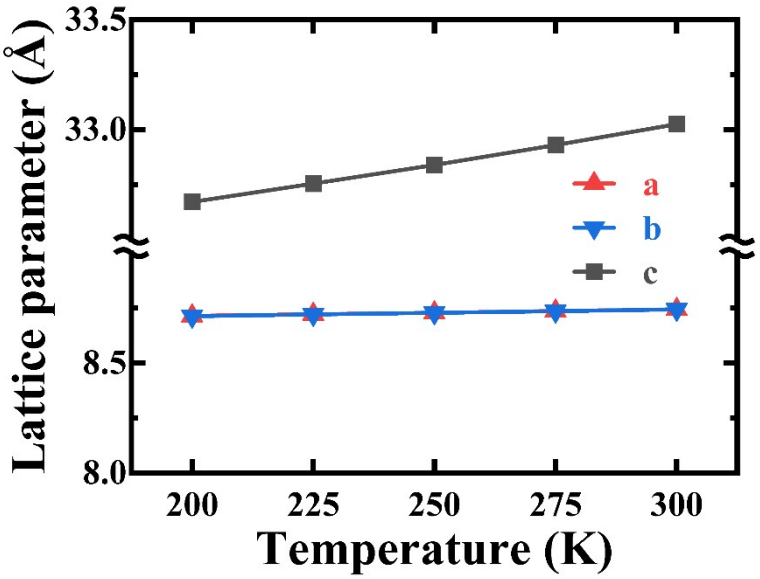

Figure S10. The lattice parameters along *a*, *b* and *c* axis which have been experimentally reported at different temperatures.

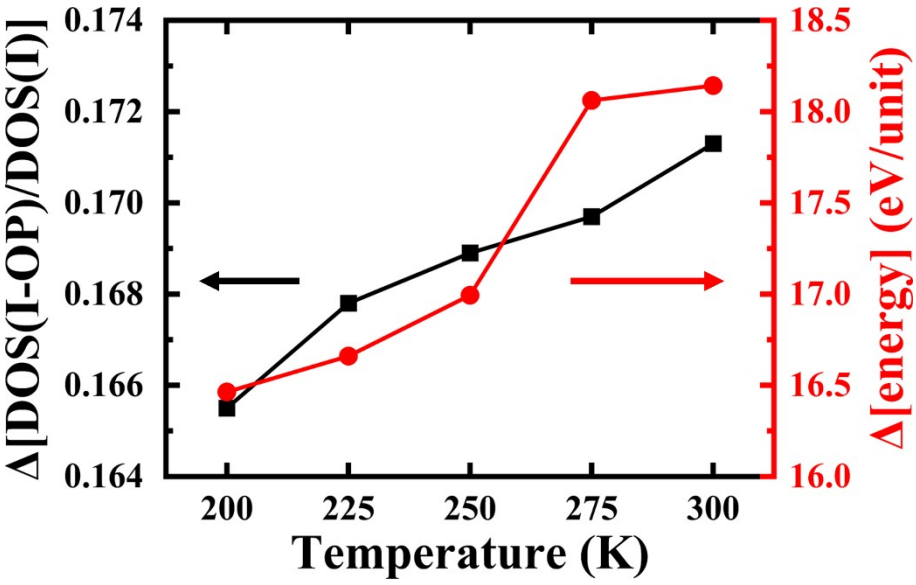

Figure S11. The differences (Δ) between the unstretched and stretched structures for the ground-state energy and for the DOS(I-OP)/DOS(I) defined in Figure 6c.

Reference

1. E. K. U. Gross and W. Kohn, *Phys. Rev. Lett.*, 1985, **55**, 2850-2852.
2. M. Marques, N. Maitra, F. Nogueira, E. K. U. Gross and A. Rubio, *Fundamentals of Time-Dependent Density Functional Theory*, Springer Science & Business Media, Berlin, 2012.
3. S. Refaely-Abramson, M. Jain, S. Sharifzadeh, J. B. Neaton and L. Kronik, *Phys. Rev. B*, 2015, **92**, 081204.
4. S. Refaely-Abramson, S. Sharifzadeh, M. Jain, R. Baer, J. B. Neaton and L. Kronik, *Phys. Rev. B*, 2013, **88**, 081204.
5. S. Refaely-Abramson, S. Sharifzadeh, N. Govind, J. Autschbach, J. B. Neaton, R. Baer and L. Kronik, *Phys. Rev. Lett.*, 2012, **109**, 226405.
6. D. Wing, J. B. Haber, R. Noff, B. Barker, D. A. Egger, A. Ramasubramaniam, S. G. Louie, J. B. Neaton and L. Kronik, *Phys. Rev. Mater.*, 2019, **3**, 064603.
7. H. Guo, X. Zhang and G. Lu, *Sci. Adv.*, 2023, **9**, eadi5404.
8. H. Guo, X. Zhang and G. Lu, *Sci. Adv.*, 2022, **8**, eabp9757.
9. H. Guo, X. Zhang and G. Lu, *Sci. Adv.*, 2020, **6**, eabc5638.
10. J. Liu, X. Zhang and G. Lu, *Nano Lett.*, 2020, **20**, 4631-4637.
11. J. Liu, Z. Li, J. Wang, X. Zhang, X. Zhan and G. Lu, *J. Mater. Chem. A*, 2020, **8**, 23304-23312.
12. J. Liu, X. Zhang and G. Lu, *J. Phys. Chem. Lett.*, 2022, **13**, 11760-11769.
13. J. Liu, Z. Li, X. Zhang and G. Lu, *npj Comput. Mater.*, 2021, **7**, 191.
14. H. Guo, X. Zhang and G. Lu, *Proc. Natl. Acad. Sci.*, 2021, **118**, e2105468118.
15. J. Liu, X. Zhang and G. Lu, *J. Phys. Chem. Lett.*, 2022, **13**, 7371-7379.
16. L. Zhang, X. Zhang and G. Lu, *Chem. Sci.*, 2021, **12**, 6073-6080.
17. J. Liu, G. Lu and X. Zhang, *J. Chem. Phys.*, 2023, **158**, 044116.
18. D. P. Chong, *Recent Advances in Density Functional Methods*, World Scientific, Singapore, 1995.
19. X. Zhang, Z. Li and G. Lu, *Phys. Rev. B*, 2011, **84**, 235208.
20. X. Zhang, Z. Li and G. Lu, *J. Phys.:Condens. Matter*, 2012, **24**, 205801.
21. K. R. Hansen, C. E. McClure, J. S. Colton and L. Whittaker-Brooks, *PRX Energy*, 2022, **1**, 013001.
22. M. Dyksik, S. Wang, W. Paritmongkol, D. K. Maude, W. A. Tisdale, M. Baranowski and P. Plochocka, *J. Phys. Chem. Lett.*, 2021, **12**, 1638-1643.
23. K. R. Hansen, J. S. Colton and L. Whittaker-Brooks, *Advanced Optical Materials*, 2024, **12**, 2301659.
24. M. S. Hybertsen and S. G. Louie, *Phys. Rev. B*, 1987, **35**, 5585-5601.
25. B. Adolph, V. I. Gavrilenko, K. Tenelsen, F. Bechstedt and R. Del Sole, *Phys. Rev. B*, 1996, **53**, 9797-9808.
26. M. Gajdoš, K. Hummer, G. Kresse, J. Furthmüller and F. Bechstedt, *Phys. Rev. B*, 2006, **73**, 045112.
27. B. Adolph, J. Furthmüller and F. Bechstedt, *Phys. Rev. B*, 2001, **63**, 125108.